Coupling the biochemical and thermochemical biorefinery platforms to enhance energy and product recovery from *Agave tequilana* bagasse

E. Emilia Rios-Del Toro[1,a], Hetian Chi[2,3,a], Víctor González-Álvarez[4], Hugo O. Méndez-Acosta[4], Jorge Arreola-Vargas[5,*] and Hao Liu[3,*]

[1]Research Center for Biotechnology and Nanotechnology, Autonomous University of Nuevo Leon. Apodaca, Nuevo León 66629, Mexico

[2]Economy & Technology Research Institute, State Grid Hubei Electric Power Company, Wuhan, 430077, China

[3]Faculty of Engineering, University of Nottingham, Nottingham, NG7 2RD, UK

[4]Department of Chemical Engineering, University of Guadalajara, Guadalajara, Jalisco, 44430, México.

[5]Department of Plant Pathology and Microbiology, Texas A&M University, College Station, 77843, Texas, USA.

[a]These authors should be considered as first authors since they contributed equally to this project and manuscript

*Corresponding authors: jorge.arreolav@tamu.edu, Liu.Hao@nottingham.ac.uk

Abstract

The tequila industry is one of the pillar industries in many regions of Mexico, bringing wealth and economic development to rural areas. However, appropriate disposal and management of the tequila manufacturing residues such as the *Agave tequilana* bagasse (TB) represent not only an environmental challenge but also an economic opportunity. Previous works have unsuccessfully applied biochemical routes for complete TB valorization. Therefore, this study aimed to achieve the full conversion of TB to energy and products by coupling the biochemical and thermochemical biorefinery platforms. The biochemical platform included acid hydrolysis of TB, detoxification of the hydrolysates with activated carbon, and two-stage anaerobic digestion of the undetoxified and detoxified hydrolysates. The energy recovery (expressed as kJ of hydrogen and methane obtained) was optimized by applying a central composite design and using both hydrolysates as substrates. Results showed that hydrogen production with the detoxified hydrolysate outperformed 2 times the undetoxified one; however, the total energy recovery (hydrogen + methane) was not favored with the detoxification process (35.04 and 37.15 kJ for the undetoxified and detoxified hydrolysate respectively), which was attributed to the robustness of the methanogenic process. Regarding the thermochemical platform, the acid hydrolysis of TB accelerated the microwave pyrolysis process and led to a higher oil yields (ca.1.5 times) with similar productions of furfural, phenol and their derivatives but significantly reduced the acetic acid formation compared to untreated TB. During the fluidized bed combustion tests, the Ca-rich TB's ash mitigated the agglomeration formation and resulted in over 900 min operation with no sign of bed defluidization. This could offer great potentials in co-combustion with other problematic biomass fuels such as wheat straw, which had a defluidization time of 60 min. Overall, these results indicate that coupling the biochemical and thermochemical platforms for *Agave*

tequilana bagasse can be a novel approach to refining gaseous and liquid products and extracting heat energy while disposing the bio-waste from tequila industry.

Keywords

Agave tequilana bagasse; lignocellulosic biomass; microwave biomass pyrolysis; fluidized bed biomass combustion; two-stage anaerobic digestion

1. Introduction

Biofuels produced from agro-industrial residues are attractive energy sources because of their potential carbon-neutral nature, low cost, abundance, and availability [1]. Nonetheless, efficient and cooperative technologies must be developed and integrated to reorient the current disposal practices in agro-industries.

In Mexico, the *Agave tequilana* bagasse (TB) is an example of a potential lignocellulosic agro-industrial residue that can contribute to enhance the energy efficiency in the tequila industry. This lignocellulosic biomass is generated after sugars are extracted from cooked agave. During this step, the TB is separated and usually inadequately disposed in agave fields while sugars are fermented to produce the worldwide recognized Mexican alcoholic beverage "tequila." According to the Tequila Regulatory Council, in 2020 alone, more than 1.4 million tons of agave were used to produce tequila, from which approximately 40% were converted to bagasse [2]. Although tequila companies have tried to implement valorization processes such as composting, little success has been achieved. Therefore, inadequate discharge of large quantities of this waste in clandestine dumps or agricultural fields has been adopted, causing the generation of odors and habitat for pests and diseases [3].

Recently, TB has been proposed as a suitable candidate for multiple biotechnological applications [4–6]. However, due to its complex lignocellulosic structure, pretreatment and

sugar hydrolysis is required prior to biofuel or chemicals production [7]. Among the evaluated depolymerization methods, dilute acid hydrolysis has demonstrated to be highly efficient for solubilization of sugars from the hemicellulose fraction. During this process two fractions are generated, a liquid fraction rich in pentoses, hexoses and furfurals, and a solid fraction constituted mainly by cellulose and lignin [8].

Previous works have demonstrated the potential of the liquid fraction (acid hydrolysate) for biohydrogen and biogas production via one or two-stage anaerobic digestion (AD) [8–10]. Nonetheless, current challenges include the removal of the toxic compounds generated during the acid hydrolysis and its effect on the two-stage AD process, as well as the optimization of key variables such as pH and substrate/inoculum ratio. These results would lay the background for the evaluation of the stability in semi-continuous or continuous systems.

Regarding the remaining fiber of the acid hydrolysis process, to the best of the authors' knowledge, there are no studies reported on its further valorization. According to a thermodynamic analysis simulation reported by Farías-Sánchez et al. (2016), the remnant TB fiber after acid and enzymatic hydrolysis is theoretically suitable for thermochemical biofuel production, with a potential hydrogen yield of 0.085 mole of H_2/g of *A. tequilana* bagasse. The most important concepts among thermochemical conversion are pyrolysis, combustion, and gasification. These processes have proved their efficiency by using vast biomass feedstocks, including other agave species [12].

Valorization of agro-industrial residues requires global approaches and integration of suitable technologies from both biorefinery platforms, biochemical and thermochemical. This hybrid technology has been recently recognized as a potential approach to valorize different biomass feedstocks worldwide, enhancing the carbon conversion and energy efficiency of the global process [13–17]. Therefore, this study presents the first effort on coupling the biochemical and thermochemical biorefinery platforms for the complete valorization of TB. A novel

integration of two-stage AD with pyrolysis and combustion was proposed for TB valorization and if proved feasible it could offer enormous environmental and economic advantages by producing gaseous and liquid products as well as heat energy while disposing the huge amount bio-waste from tequila industry.

Via the biochemical platform, hydrogen and methane productions were optimized by applying a central composite design (CCD) to the two-stage AD of detoxified and undetoxified acid hydrolysates of TB. Regarding the thermochemical process, pyrolysis was firstly evaluated for both TB and acid pretreated bagasse (H-TB) to verify the pyrolysis rate as well as the bio-oil products. Then, the combustion test confirmed the suitability of TB as a quality biomass fuel for fluidized bed combustion systems. A final analysis on the integration of both biorefinery platforms was conducted and discussed.

2. Materials and Methods

2.1 Materials

TB was kindly supplied by Casa Herradura distillery, located in Amatitan, Jalisco, Mexico. Prior to its use, a single batch of TB was sun-dried and ground to an average particle size of 1 cm. The lignocellulosic composition of this TB batch was: 12.44 ± 1.43% hemicellulose, 55.08 ± 3.92% cellulose, and 13.12 ± 1.99 % lignin.

The inoculum used for the two-stage AD was anaerobic granular sludge collected from a full-scale UASB (up-flow anaerobic sludge blanket) reactor treating tequila vinasses. For hydrogen production, the inoculum was thermally treated at 104 °C for 24 h and then ground in a mortar and sieved with a mesh of 850 μm [18]. Both thermally pretreated and non-pretreated inocula were stored at 4 °C.

During thermochemical conversion, wheat straw (WS1) and wheat straw with 1.5 wt% lime addition (WS2) were also evaluated to compare with TB. Besides, quartz sand (Garside

14/25) with a particle density of 2655 kg/m^3 and a grain size below 1.0 mm (D50=0.78 mm) was used as the bed material of the bubbling fluidized bed combustor that was used to conduct the combustion tests.

2.2 Biochemical platform

2.2.1 Acid hydrolysis and detoxification process

Acid hydrolysis of TB and detoxification of the hydrolysates were performed according to a previous work [19]. Briefly, 30 g of TB were suspended in 600 mL 1.9% HCl solution in 1 L corning® glass bottles and subjected to hydrolysis in an oven (BINDER®, FED Avantgarde Line 260) at 130 °C for 192 minutes (including 60 min to allow the solution to heat up to 130 °C and 132 min of hydrolysis time). Before the bottles (with TB and 600 mL of 1.9% HCl solution) were introduced in the oven, they were shaken manually to ensure the bagasse was completely impregnated with acid solution. After 192 min, the bottles were cooled down at room temperature and the liquid (acid hydrolysate) was decanted and filtered through cheese cloth. The bottles were re-filled with 600 mL of distilled water and 1 mL of 50% NaOH solution and again manually shaken. Then, the biomass was washed with 1-2 L of distilled water until neutrality. Finally, the remaining fiber (H-TB) was filtered through cheese cloth, dried at 60 °C overnight and stored in the dark for thermochemical analyses.

The hydrolysate was detoxified by using coconut shell activated carbon. Briefly, the acid hydrolysate was mixed at 150 rpm with coconut shell activated carbon at a concentration of 1% w/v for 20 min at room temperature. After the detoxification process, the activated carbon was removed by filtration through filter paper Whatman®, No. 42, and the liquid fraction (detoxified hydrolysate) was stored at 4 °C in the dark. The main composition of the undetoxified and detoxified hydrolysates is presented in Table S1.

2.2.2 Two-stage AD of the detoxified and undetoxified hydrolysates

Two-stage AD was employed to convert sugars from both hydrolysates to hydrogen and methane. Optimization of two of the most important variables (chemical oxygen demand (COD) and pH) for this two-stage process was performed aiming for the maximization of energy recovery (expressed as kJ of hydrogen and methane produced). A CCD was used for the optimization because this experimental design is the most renowned design for optimization of significant variables [10]. This design optimizes response variables through sequential experimentation, using second order models to predict the response variable (equation 1). Data analysis, response surface plots, and analysis of variance (ANOVA) were performed using the software Statgraphics centurion XV (Statpoint, Technologies, Inc. USA).

$$Y = \beta_{\circ} + \sum \beta_{i} x_{i} + \sum \beta_{ii} x_{i}^{2} + \sum\sum \beta_{ij} x_{i} x_{j} + \varepsilon \qquad \text{Eqn. 1}$$

where β_0 is the constant coefficient, β_i is the linear coefficient, β_{ii} is the quadratic coefficient, β_{ij} is the interaction coefficient, Y is the response variable, x represents the independent variables that influence the response variable, and ε is a random error term that accounts for the experimental error in the system.

Hydrogen and methane production assays were carried out in an automatic anaerobic methane potential test system (AMPTS II-Bioprocess Control AB, Lund Sweden) at pH and COD values suggested by the CCD (Tables S2 and S3).

The AMPTS system consists of 15 reactors of 500 mL of capacity, CO_2 traps and a flow meter unit. This equipment allows to measure and record automatically, at normal temperature and pressure conditions, the biogas flow generated in the reactors. To quantify the volume of H_2 or CH_4 produced in the biogas accurately, CO_2 traps were placed between the reactors and the flow meter unit. These traps contained a 3N NaOH solution with

thymolphthalein as an indicator. Each reactor was inoculated with 10 g of volatile suspended solids (VSS)/L and fed with 360 mL of hydrolysate (undetoxified or detoxified). The first stage was inoculated with thermally pretreated sludge to favor hydrogen production and inhibit methane production while the second stage was inoculated with fresh sludge and fed with the effluent of the first stage at adjusted pH 7.5. At the beginning of the first stage, the initial pH and COD were adjusted according to the CCD, and the reactors were flushed with nitrogen gas to ensure anaerobic conditions. All the experiments were performed in triplicate at 37 °C with a constant agitation of 150 rpm.

2.3 Thermochemical platform

2.3.1 Microwave pyrolysis

Three biomass samples (TB, H-TB; and WS1 for comparison purposes) were pulverized down below 75µm grain size to increase the homogeneity of the samples in the microwave field and densified by a pellets press die under 2 tons of pressure to have a 20mm long and 13mm diameter biomass pellet with weight around 3.3g.

The experimental rig mainly includes a 2kW microwave generator (SAIREM, France), a pyrolysis setup, auxiliary water and nitrogen gas supply, and a computer data logger as previously reported [20]. The schematic of the rig is shown in the supplementary data Fig. S1. The microwave generator was operated at 2.45 GHz frequency, and three levels of power input were chosen at 500W, 750W, and 1000W. The residence time was initially determined by thermal runaway at 500W. It turned out that the H-TB has a reasonable operation time of 120s before hitting thermal runaway. Thus, to facilitate the comparisons of the pyrolysis outcomes and to protect the reactor, a fixed energy input of 60kJ (=500W*120s) was used for all the tests, and the residence time at each power input level can be determined, i.e., 120s for 500W; 80s for 750W; 60s for 1000W. Details of the thermal runaway are shown in Fig. S2.

The biomass pyrolysis took place in a customized quartz tube (30mm i.d. and 360mm in length), and the biomass pellet was placed in the center of the tube held by a porous quartz gas distributor. To maintain the anoxic conditions, nitrogen gas was injected into the system through the bottom at a 2mL/min flow rate. A 5min purging was performed to maintain an inert atmosphere before the test and cool down the reactor after the test. At the beginning of the test, the microwave tuning was performed to maximize the absorbed power and log forward and reflected power. During the test, liquid products were captured by the Schlenk flask in an ice bath combined with an extra condenser. The non-condensable gas products were emitted through the extraction system.

Once the reactor cooled down, the solid products were removed from the tube, dried, and weighed. The total pyrolysis yield was determined following equation 2 [21]:

$$Total\ pyrolysis\ yield\ (\%) = 100\% - (\frac{weight\ of\ the\ solid\ residue}{weight\ of\ the\ sample} \times 100\%) \qquad \text{Eqn. 2}$$

2.3.2 Bubbling fluidized bed combustion tests

The 20kW$_{th}$ bubbling fluidized bed (BFB) apparatus (Fig. S3) was described in detail in our previous publication [22]. Briefly, the apparatus mainly includes a 20kW$_{th}$ BFB combustor and the auxiliary systems for air supply, biomass feeding, gas analysis, and data monitoring and recording. The fluidization air, 15 m^3/hr at ambient temperature and atmospheric pressure (ATAP) is supplied from a compressor, heated up by an electric pre-heater before the plenum, and then fed into the combustor through a porous stainless gas distribution plate (100 μm pore size and 12 mm thickness). Two half-cylindrical electric heaters are used to pre-heat the combustion zone. Once the bed temperature reaches about 500°C, the biomass pellets are fed into the combustor at the location just above the gas distribution plate together with an air flow of 5.7 m^3/hr (ATAP) which is used mainly for the prevention of biomass backfiring to

the fuel hopper. Therefore, a total air flow of 20.7 m^3/hr (ATAP) is supplied for the combustion purposes, and the excess O_2 in the flue gas is controlled between 4% and 5% by maintaining the fuel supply at a suitable feeding rate.

The highest bed temperature with the combustion tests of WS1 pellets could reach about 880°C before the bed defluidized as a result of severe bed material agglomeration. The highest bed temperatures with the combustion tests of TB and WS2 pellets reached 900°C with the bed materials still properly fluidized. In order to protect the BFB combustor, these bed temperatures were brought down to about 880°C for the remaining period of each test by inserting the U-shape heat extraction probe to the combustor. The temperature levels tested (880°C - 900°C) in this study represent the highest operation temperatures for most industrial-scale fluidized bed boilers, including those of supercritical circulating fluidized bed power plant boilers [23].

The initiation of the bed defluidization was detected and judged by the divergence of the decreasing bed temperature and the increasing freeboard temperature, and the flattening of the bed pressure drop fluctuations. The pressure drop profile across the BFB combustor used in this study was typically fluctuating between 15-50 mbar due to the fluidization of the bed particles. A sudden drop in the bed temperature, combined with an increase in freeboard temperature and the flattening of the bed pressure drop fluctuations, indicated the defluidization of the bed materials. Once the bed was judged to have defluidized, the fuel feeding was stopped immediately. Then, the combustor was let to cool down before the used bed materials and the fly ash samples could be collected.

2.4 Analytical methods

The lignocellulosic composition of TB and H-TB was determined by using a semiautomatic ANKOM fiber analyzer as previously reported [19]. TB and H-TB were also characterized by

proximate analysis following the ASTM E871-82 for moisture, ASTM E1755-01 for ash, and ASTM E872-82 for volatile matter determination. The ultimate analysis was performed based on the pre-dried fuels (at 105°C) using *Leco CHN-628* integrated with *628-S.* Fuel ash compositions were acquired by SEM/EDX (JEOL 6490LV). Proximate and ultimate analyses and low-temperature ash composition of the fuels (including WS for comparison) and the bed materials (Quartz sand) are presented in **Table 1**.

Table 1. Properties of the biomass fuels and bed material.

	TB	**H-TB**	**WS1**[c]	**WS2**[d]	**Quartz sand**
Proximate analysis (wt%)					
Moisture (ar [a])	11.28	5.48	6.15	8.44	-
Ash (db [b])	6.79	0.93	7.01	3.42	-
Volatile matter (db)	85.75	84.09	73.20	78.85	-
Fixed carbon (db)	7.46	14.99	19.79	17.73	-
Ultimate analysis (wt%, db)					
Carbon	40.05	47.62	42.61	42.79	-
Hydrogen	6.36	6.49	6.34	6.34	-
Nitrogen	0.55	0.65	0.43	0.42	-
Sulphur	<0.01	<0.01	<0.01	0.05	-
Oxygen (by difference)	46.25	44.31	43.61	46.98	-
HHV (kJ/g, db estimate)	16.54	19.66	17.68	17.48	
Ash/Quartz sand composition (% wt)					
SiO_2	1.52	16.26	44.00	35.20	96.67
K_2O	1.05	2.55	14.90	14.00	0.01
CaO	49.17	27.20	6.65	13.70	0.01
P_2O_5	0.73	1.05	3.63	3.98	-
SO_3	0.66	7.45	1.90	2.40	-
MgO	2.52	5.92	2.00	2.60	<0.01
Na_2O	0.22	11.23	-	-	0.03
Cl	-	0.52	0.88	0.34	-
Fe_2O_3	0.27	1.18	0.26	1.53	2.40
Al_2O_3	0.45	3.53	-	1.70	0.33
Others	-	0.45	0.13	0.40	0.55
Ash fusion temperature (℃)					
DT	815	1060	798	810	-
ST	1380	1160	1025	1045	-
HT	1435	1185	1225	1200	-

FT	1455	1195	1260	1230	-

[a] As received; [b] Dry base; [c]WS1: Wheat straw, [d]WS2: Wheat straw with 1.5 wt% lime. *TB: Agave tequilana bagasse; H-TB: acid pretreated bagasse.* Deformation temperature (DT); Sphere temperature (ST); Hemisphere temperature (HT); Flow temperature (FT). HHVs are estimated according to the correlation previously reported [24].

Undetoxified and detoxified hydrolysates were characterized in terms of i) total sugars by the phenol-sulfuric acid method [25]; ii) monosaccharides and potential inhibitory compounds such as 5-hydroxymethylfurfural (HMF) and furfural by HPLC; iii) COD by using a HACH digester DRB200 and spectrophotometer DR2800; iv) volatile fatty acids such as formate, acetate, propionate, butyrate, isobutyrate, valerate, and isovalerate by HPLC. COD and HPLC analyses were also used to characterize the fermentation byproducts as described elsewhere [19]. Hydrogen and methane produced during the two-stage AD are automatically recorded at standard temperature and pressure by the AMPTS II.

The oil products from the microwave tests were collected by repeatedly washing with acetone, and then the acetone was removed in an evacuated oven to quantify the oil products derived from each test. The oil composition was analyzed using GC-MS in full scan mode (m/z 50-450) with a Varian CP-3800 gas chromatograph, interfaced to a Varian 1200 mass spectrometer (EI mode, 70 eV). The separation was made using a ZB-1701 fused silica capillary column (60 m x 0.25 mm i.d., 0.25 mm thickness), with helium as the carrier gas, and an oven program of 50°C (hold for 2 min) to 300°C (hold for 33 min) at 5°C/min ramping rate.

In the BFB combustion tests, the agglomerates were assumed to be the particles more significantly larger than the original sand particles' top size and were collected by sieving the used bed materials with a 1.18 mm sieve. Both the agglomerates and the fly ash samples were ground down to a grain size between 10-20 μm for the XRD (BRUKER D8 Da Vinci) analysis. Selected agglomerates were embedded in epoxy resin, then cut and polished, and

coated with 10 nm carbon for the SEM/EDX (JEOL 6490LV, FEI QUANTA 600) analysis on the cross-section. The exhaust gas composition at the exit of the BFB combustor was continuously analyzed by online gas analyzers: O_2, CO_2, and CO concentrations were measured by an easy line continuous gas analyzer (ABB, EL3020); NO_x concentration was measured by a chemiluminescent NO_x analyzer (Horiba VA-3000). The fuel ash and elutriated solids captured by the cyclone were collected after each test day for further off-line analysis.

3. Results and discussion

3.1 Characterization of fibers (TB and H-TB) and acid hydrolysates

Table 1 shows the properties of the materials used during this study. Overall, TB and H-TB contained more volatile matter than wheat straw (WS), and the acid pretreatment reduced significantly the content of ashes in TB. Previous reports [4,26] have demonstrated that pretreatment of TB reduces the content of calcium oxalate crystals that are the main inorganics found in agave species, agreeing with our observations. In fact, calcium was detected in the hydrolysates (1.06 ± 0.01 g/L, Table S1) confirming the release of calcium oxalates from TB during the acid pretreatment. Regarding this liquid fraction, Table S1 shows that both undetoxified and detoxified hydrolysates were mainly constituted by sugars. Xylose was the main monosaccharide followed by galactose; however, presence of oligosaccharides is presumed due to the difference between the sum of monosaccharides and the total sugar concentration. High xylose content in the hydrolysates is due to the acid hydrolysis of xylan, which is initiated by protonation of the glycosidic linkage. However, deacetylation and further dehydration of sugars result in generation of toxic byproducts such as acetic acid and furans [27]. These compounds were detected in the hydrolysate but mostly removed during the detoxification process, highlighting the high efficiency of this detoxification process to

remove toxic compounds from acid hydrolysates while maintaining high concentrations of sugars [19].

3.2 Energy recovery from hydrolysates of TB: Biochemical platform

Our previous research had demonstrated the potential of detoxified acid hydrolysates of TB for hydrogen production [19]. However, during dark fermentation processes most of the organic matter is converted to fatty acids, leading to waste generation that could be further upgraded to methane and other products. Therefore, during this study, both undetoxified and detoxified hydrolysates were used as substrates for hydrogen and methane production via two-stage AD system. The energy recovery (measured as kJ of hydrogen and methane produced) was optimized by using a CCD coupled to a response surface methodology where COD and pH were the independent variables.

Responses obtained from both CCDs are presented in Tables S2 and S3. The undetoxified hydrolysate was evaluated with a wide range of COD values, and pH values close to neutrality. Results showed that at high COD values the total energy recovery decreased significantly, which is attributed to high production of fatty acids that lead to acidification and instability of the AD process [28]. Thus, for the detoxified hydrolysate the COD range was reduced and the pH was slightly increased by 0.5 units (Table S3). **Table 2** shows that COD was the only significant variable (p-value = 0.0149 and 0.0014 for the undetoxified and detoxified hydrolysate, respectively), evidencing that pH does not affect energy recovery and no interaction between variables was present within the evaluated ranges.

Table 2. ANOVA for the responses obtained from the CCD by using both hydrolysates as substrate.

Undetoxified hydrolysate					
Source	**Sum of Squares**	**DF**	**Mean Square**	**F-value**	**P-value**
A: COD	120.84	1	120.84	16.75	0.0149
B: pH	0.46	1	0.46	0.06	0.8128
AA	481.80	1	481.80	66.77	0.0012
AB	1.21	1	1.21	0.17	0.7032
BB	10.75	1	10.75	1.49	0.2891
Total error	28.86	5	7.21		
Total	683.38	10			
Detoxified hydrolysate					
Source	**Sum of Squares**	**DF**	**Mean Square**	**F-value**	**P-value**
A: pH	1.92	1	1.92	0.05	0.8299
B: COD	1011.02	1	1011.02	26.07	0.0014
AA	2.58	1	2.58	0.07	0.8037
AB	2.32	1	2.32	0.06	0.8138
BB	270.03	1	270.03	6.96	0.0335
Total error	271.51	7	38.78		
Total	1571.12	12			

Where DF = degree of freedom

Responses obtained from both CCDs were subjected to analysis using the response surface methodology. Equations 3 and 4 show the second-order models that accurately represent the responses obtained by the undetoxified and detoxified hydrolysates, respectively. The coefficients of determination (R^2) for equations 3 and 4 were 0.80 and 0.82, indicating appropriate fitting to experimental data with 95% confidence (p-value=0.0001).

Energy recovery (kJ) =

$$-233.5 + 4.3*COD + 69*pH - 0.33*COD^2 + 0.22*COD*pH - 5.05*pH^2 \quad \text{Eqn. 3}$$

Energy recovery (kJ) =

$$136.152 - 45.1719*pH + 19.8185*COD + 2.43817*pH^2 + 0.7617*pH*COD - 1.55761*COD^2 \quad \text{Eqn. 4}$$

Second order models presented in Eqn. 3 and Eqn. 4 were used to generate the response surface charts (**Fig. 1**). **Fig. 1** shows that the highest energy recovery (hydrogen + methane) was found to be close to the center points for both hydrolysates. The optimal conditions suggested for the undetoxified hydrolysate were 7.02 of pH and 8.84 g/L of COD; for the detoxified hydrolysate the optimal conditions were slightly lower (pH= 6.80 and COD= 8.02 g/L). These conditions were evaluated experimentally (**Table 3**), obtaining hydrogen energy recoveries of 3.11 and 6.34 kJ for the undetoxified and detoxified hydrolysates, respectively. This agrees with our previous observations [19] and confirms that detoxification of acid hydrolysates is efficient to remove toxic compounds that affect fermentative hydrogen production.

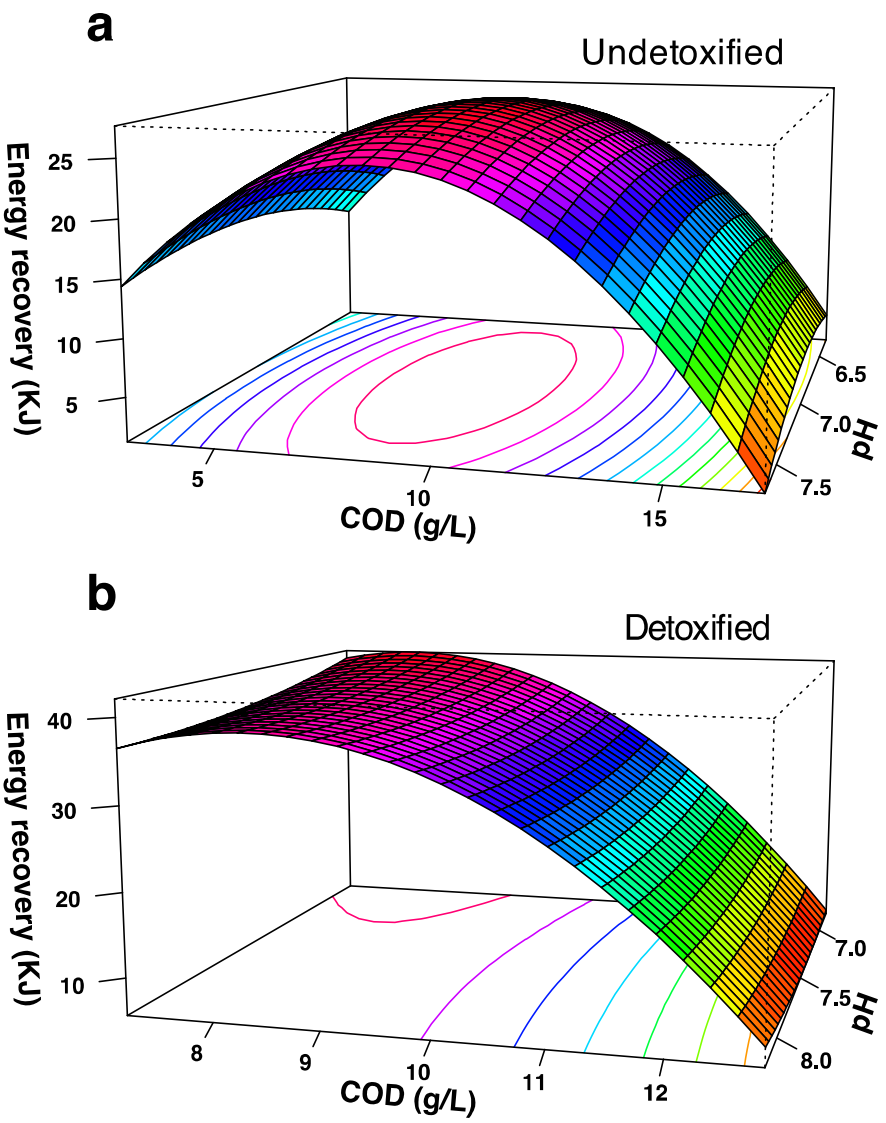

Fig. 1 Response surface for energy recovery from the two-stage anaerobic digestion of *A. tequilana* bagasse at different pH and COD concentrations. a) Undetoxified hydrolysate and b) detoxified hydrolysate.

Table 3. Comparative performance of both hydrolysates under optimal conditions of pH and COD.

Parameter	**Undetoxified hydrolysate**	**Detoxified hydrolysate**
COD (g/L)	8.84	8.02

pH	7.02	6.80
Yield-H_2 (mol H_2/mol glucose)	1.11 ± 0.05	1.81 ± 0.14
Yield-CH_4 (L CH_4/g COD)	0.20 ± 0.02	0.18 ± 0.05
Energy recovery-H_2 (kJ)	3.11 ± 0.15	6.34 ± 1.2
Energy recovery-CH_4 (kJ)	31.93 ± 0.5	30.81 ± 1.7
Total energy recovery (experimental values (kJ))	35.04	37.15

At optimal conditions, the energy recovery as methane was 31.93 kJ with the undetoxified hydrolysate and 30.81 kJ with the detoxified hydrolysate (**Table 3**). Interestingly, the energy recovery with the undetoxified hydrolysate resulted in slightly higher than the detoxified hydrolysate. Previous studies have reported that anaerobic digestion is more robust and can have higher inhibition thresholds for toxic compounds generated during lignocellulose pretreatment compared to dark fermentation processes [29,30]. Moreover, the main substrate for methanogenic communities is acetate, which is one of the main organics removed by the detoxification process. We have hypothesized that these latter points may have impacted the energy recovery during the methanogenic process.

Even though the hydrogen energy recovery was 2-fold increased by the detoxification process, the total energy recovery was not significantly different between the two substrates (35.04 kJ for the undetoxified and 37.15 kJ for the detoxified hydrolysates, *p*-value> 0.05). This is explained by the low energy recovered as hydrogen compared to that as methane. The highest hydrogen yield stoichiometry shows that for every mole of assimilated glucose up to 4 moles of hydrogen and 2 moles of acetate are produced [31], which is equal to recover 8 electron equivalents as hydrogen from originally 24 electron equivalents in glucose; i.e. recovering a maximum of 33.33% of energy as hydrogen and leaving 66.66% as acetate [32]. Moreover, in mixed cultures fed with complex substrates, this reaction occurs simultaneously

with many others [31], producing multiple byproducts and decreasing the hydrogen yield even more to values under 2 moles (**Table 3**). It is important to highlight that in the present study most of the byproducts generated during the hydrogenogenic stage were converted to methane during the methanogenesis process (Fig. S4).

The total energy recovery from both hydrolysates represents an energy yield of 5 ± 0.03 kJ/g of bagasse, which is equivalent to approximately 30% of the bagasse's initial energy by taking into account the estimated higher heating value (HHV) of TB presented in Table 1, 16.54 kJ/g. This estimated HHV here is similar to the previous value of 16.35 kJ/g reported by Liñán-Montes et al. (2014). Meanwhile, the energy yield is similar to previous reports using other feedstocks such as sugarcane bagasse (4.8 kJ/g bagasse) [34]. However, previous reports with TB have achieved 9.2 kJ/g bagasse (Montiel Corona and Razo-Flores., 2018) and 8.2 kJ/g bagasse (Arreola-Vargas et al., 2016a). Nonetheless, these latter values were obtained by using enzymatic hydrolysates as substrate, which involves the use of cellulases that are more expensive than mineral acids.

3.3 Thermochemical analyses of H-TB

As a result of the acid pretreatment, a fiber rich in cellulose (64.36 %) and lignin (20.81 %) was generated; the hemicellulose fraction was completely hydrolyzed. The second part of this work was focused on the evaluation of TB and its residual fiber after acid pretreatment (H-TB) aiming at the integration of different biorefinery approaches for the full utilization of TB. As mentioned above, WS was used for comparative purposes.

3.3.1 Pyrolysis yield

At the end of each pyrolysis test, the oil products were collected by acetone, which was later removed in an evacuator at ambient temperature to acquire the weight of the oil products. The

gas proportions were calculated by deduction. As shown in **Fig. 2**, at 500 and 750W of incident power, H-TB obtained the highest oil yield while TB obtained the lowest, suggesting significant benefits of the acid pretreatment, such as (1) the removal of the ash increased the purity of the fuel which is in favor of the pyrolysis [35], and (2) the degradation of lignocellulose could accelerate the pyrolysis process [36].

Comparing the product yields at different power levels, the liquid products of TB and H-TB decreased with the increasing of power inputs, but the proportions of WS pyrolysis products remained more or less constant for all power levels (**Fig. 2**). Only a slight decrease in the WS-derived liquid product was observed when increasing the incident to 1000W. This could be caused by the lower volatile matter (VM) but higher fixed carbon (FC) in WS (**Table1**), which made the fuel not as sensitive as the other samples in terms of absorbing power by FC and forming liquid products due to VM.

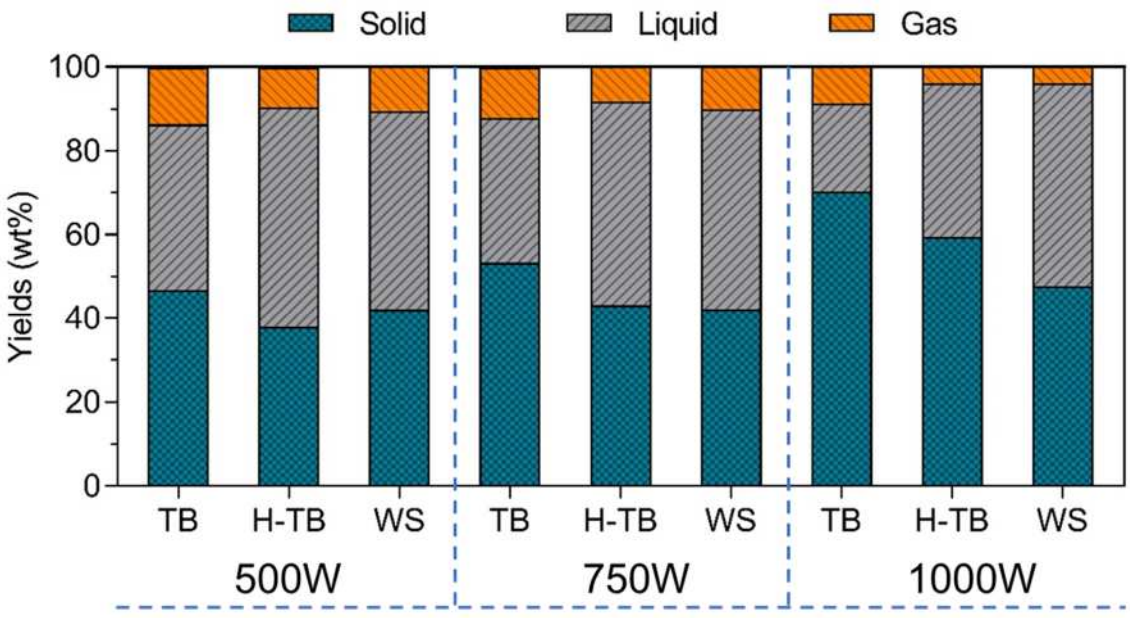

Fig. 2 Solid, liquid and gas yields of different biomasses at different incident power levels during pyrolysis.

3.3.2 Oil product compositions

The chromatograms of the acetone soluble fractions produced by selective oil products are shown in **Fig. 3**, and the relative concentrations of the compounds derived from all the bio-oil products are shown in **Table 4**. It is important to notice that not all bio-oil components could be included since polar and high molecular weight components were not extracted/detected [37].

TB and H-TB gave similar chromatograms (**Fig. 3** a, b) with the significant compounds identified as furfural and phenol and their derivatives. The substantial difference was the formation of abundant acetic acid from TB but not from H-TB. This is consistent with the studies of fast biomass pyrolysis [38] and the hydrothermal conversion of biomass [39,40]. Furthermore, the acetic acid production mainly depends on 1) the hemicellulose content in the biomass, which was removed by the acid pre-treatment [36]; and 2) the presence of a wet atmosphere. In this study, no moisture was added into the system, thus with higher moisture content in the sample (**Table 1**), the pyrolysis of TB could also lead to a higher concentration of acetic acid than that of H-TB.

The chromatogram of WS1 (**Fig. 3** c) was distinguishable from those of TB and H-TB oil products. In general, the chemical composition of the WS1 pyrolysis is consistent with previous studies [41]. The presence of ethyl-phenol and its derivatives was observed only in the WS1 derived bio-oil, and the acetic acid production was much higher than that of H-TB but lower than that of TB.

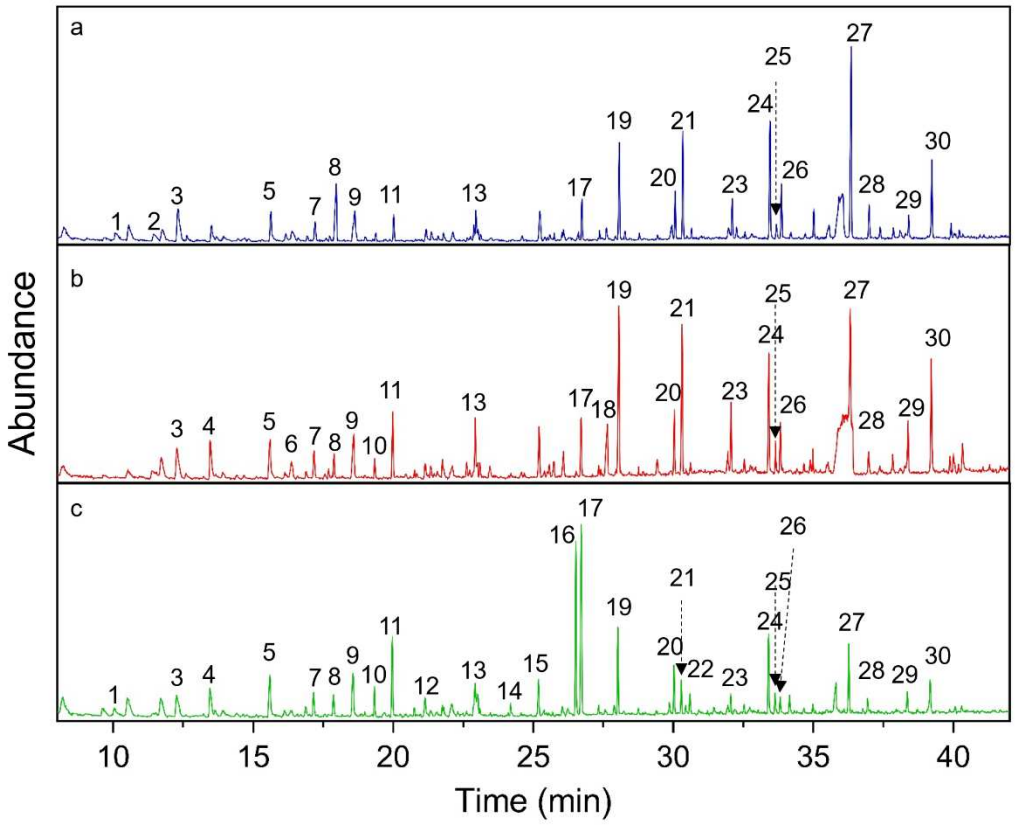

Fig. 3 Chromatogram of acetone soluble fractions from selective oil products: (a) TB at 500W; (b) H-TB at 500W; (c) WS at 500W.

Table 4. List of major compounds identified by the GC-MS chromatograms with the relative concentration

		Relative concentration (%)								
		500W power input			750W power input			1000W power input		
Peak	Compound	TB	H-TB	WS	TB	H-TB	WS	TB	H-TB	WS
1	Acetic acid	38.71	5.05	20.87	31.95	4.96	15.41	40.45	4.97	19.20
2	2-propenoic acid	0.86	-	-	2.27	-	-	1.53	-	-
3	3-furaldehyde	4.51	5.18	3.65	3.71	5.61	3.77	4.32	7.40	3.96
4	2-Furanmethanol	-	4.12	3.01	0.00	4.01	3.26	-	4.41	2.85
5	1,2 cyclopentanedione	2.52	4.33	4.14	2.84	4.01	4.68	2.26	3.90	4.14
6	2-furancaboxaldehyde,5-methyl	-	2.36	-	-	2.49	-	-	2.62	-
7	2-furanone	1.33	2.35	1.98	1.34	2.25	1.87	1.06	2.24	1.72
8	Oxazolidine 2,2-dithyl-3-methyl	4.47	1.57	1.51	5.06	1.58	1.43	4.90	2.09	1.26
9	2-cyclopenten-1,one-2hyroxy-3-methyl	3.14	4.62	4.09	3.44	4.80	4.35	2.57	4.58	3.90
10	phenol	-	1.11	1.67	0.00	1.07	1.60	0.00	0.64	1.26
11	phenol, 2-methoxy	1.39	4.39	4.68	1.37	4.25	5.03	0.94	3.56	5.07
12	2-cyclopenten-1,one,3-ethyl-2-hydroxy	-	-	1.31	-	-	1.42	-	-	1.31
13	phenol,2-methoxy-4-methyl	0.94	3.04	1.71	0.80	3.23	1.94	0.93	1.95	1.73
14	phenol, 3-ethyl	-	-	0.51	-	-	0.95	-	-	0.55
15	phenol, 4-ethyl-2-methoxy	-	-	2.35	-	-	2.63	-	-	2.32
16	Benzofuran, 2,3,-dihydro	-	-	9.95	-	-	10.64	-	-	10.81
17	Ethanone, 1-(2-hydroxy-5-methylphenyl)	1.89	3.28	11.42	2.25	3.35	11.73	2.11	3.34	11.74
18	2-furan carboxaldehyde, 5-(hydroxymethyl)	0.00	5.15	0.00	0.00	6.37	0.00	0.00	6.61	0.00
19	phenol, 2,6-dimethoxy	4.82	11.13	5.21	5.18	12.25	5.53	3.33	9.79	5.32
20	phenol, 2-methoxy-4-(1-propenyl	2.29	3.32	2.58	2.79	3.32	2.84	1.47	3.54	2.84
21	1,2,4-trimethoxybenzene	5.29	9.36	1.61	5.17	9.28	1.80	3.23	7.10	1.79
22	benzaldehyde, 3-hydroxy-4-methoxy	-	-	1.25	-	-	1.41	-	-	1.33
23	4-ethylbiphenyl	1.68	3.75	1.10	1.53	3.80	1.28	0.98	3.26	0.97
24	Ethanone, 1-(3,4-dimethoxyphenol)	6.24	7.33	4.91	7.01	7.30	5.06	5.54	7.19	4.98
25	Propanone, 1-(4-hydroxy-3-methoxyphenyl)	0.64	1.71	1.31	0.73	1.99	1.28	0.92	1.90	1.32
26	2,6-Dimethylphenol	2.74	2.87	0.89	3.05	2.96	1.06	3.12	3.20	1.07
27	3,5-Dimethylphenol	10.25	1.72	3.72	11.60	1.19	4.29	11.88	1.97	3.98
28	Benzaldehyde, 4-hydroxy-3,5-dimethoxy	1.67	1.63	0.64	2.10	1.11	0.83	2.38	1.88	0.72
29	Ethanone, 1-(4-hydroxy-3.5-dimethoxyphenyl)	0.93	2.90	1.23	1.20	2.95	1.31	1.12	3.29	1.20
30	1-butanone,1-(2,4,6-trihydroxy-3-methylphenyl)	3.69	7.71	2.72	4.64	5.85	2.59	4.96	8.57	2.69

3.3.3 BFB Combustion profiles

The main operation conditions and observations for each BFB combustion test are shown in **Table 5**. Combustion tests of TB, H-TB and WS were attempted to evaluate another alternative for valorization of the agave residue as well as to compare with a typical biomass fuel. Interestingly, due to its physicochemical characteristics of H-TB, it was not possible to obtain adequate H-TB pellets for the BFB combustion tests. This was due to the fact that the acid hydrolysis treatment of TB removed all of the hemicellulose and degraded the in-situ lignocellulose structure which is a natural binder for biomass pelletization. Moreover, the pelletization of H-TB also failed even with the addition of an artificial binder up to 20 wt% and using an industrial pelletization machine. Thus, we have hypothesized that if TB can be successfully combusted then H-TB should have little or no operation problems, since the acid pre-treatment removed most of the ash content present in the raw TB. Nonetheless, further investigations on the H-TB pelletization and combustion are encouraged.

Table 5. Detailed operation conditions of the combustion tests.

Test	Fuel	Bed temperature (°C)	Fuel additive	Defluidization time (min)	Observations
R#1	WS1	870	N/A	54	Defluidized before stable combustion being achieved
R#2	WS2	900	1.5 wt% Lime	>900	Stable combustion being achieved
R#3	TB	900-870	N/A	>900	Stable combustion being achieved

Using TB as a biomass fuel for fluidized bed combustion systems is a relatively new approach, and experimental research is needed to have a comprehensive understanding of TB as a biomass fuel. Compared to high quality biomass fuels, WS has been identified as a problematic fuel in fluidized bed combustion systems due to the high potassium and chlorine

contents in the fuel [42,43]. Previous studies have demonstrated that WS1 suffered from rapid bed defluidization problems at the high end of typical fluidized bed combustion temperatures (ca. 870℃), and a 1.5 wt% lime addition to fuel successfully extended the WS1 defluidization time from 60 min to above 900 min [44]. However, the high-temperature combustion performance of TB remains unclear in FB systems. If TB has little or no operational problems at the high end of typical FB combustion temperatures (800-900℃), this biomass could potentially be used as an alternative to the premium quality wood pellets used in large-scale FB combustion power plants.

Fig. 4 shows the combustion profiles, including temperature distributions, bed pressure drops, and significant gas emissions. Combustion tests with TB and WS2 shown in **Fig. 4** a, c were conducted on different days (i.e., shifts) as continuous tests outside normal working hours were not permitted based on the consideration of safety and researchers' well-being. Each of these tests was restarted and continued on the next shift using the same bed materials used in the previous shift.

Fig. 4 b illustrates the operation profiles of WS1 combustion test. Bed defluidization was observed within 60 min after feeding started as the bed temperature dropped which was accompanied with the increase of the upper zone temperatures (T4 and T5) while the pressure variance flattened. This phenomenon was not observed during the TB and WS2 tests even after 900 min (accumulated) combustion tests. Moreover, burning WS1 led to the maximum bed temperature at 877°C, whereas the maximum bed temperature reached when firing TB or WS2 was higher (900°C).

Due to the small variations in fuel feeding rates caused by the biomass fuels' heterogeneous nature and the volumetric feeding, rather than gravimetric feeding of the screw feeder, the excess oxygen concentration in the dry flue gas varied between 4 and 5%. The same excess oxygen concentration was controlled by adjusting the fuel feeding rate to achieve similar

overall combustion conditions across the three tests. Therefore, this facilitated the parallel comparisons of the CO and NO_x emissions among the three fuels' combustion: (1) the CO concentration in the flue gas of TB combustion was slightly lower than that derived from WS1 and WS2 combustion; (2) the NO_x concentration in the flue gas of WS1 combustion was increasing (until the bed defluidized) due to the constant climbing of the bed temperature (**Fig. 4** b) – the highest NOx concentration measured before bed defluidization was about 340ppm. Both the NOx emissions of TB and WS2 combustion were much more stable as a result of stable combustion had been established in the BFB combustor and there was no defluidization occurring during the tests. It can be seen clearly from **Fig. 4** a and c that the TB-derived NO_x emissions (ca.280 ppm) were higher than those (ca. 170 ppm) of WS2 combustion. TB contains higher fuel-N than WS2 (**Table 1**) and hence when combusted under similar conditions, TB combustion is expected to emit higher NOx. Co-firing TB and WS1 may have great potentials in FB systems considering the resultant moderate NO_x emission and the possibility of significantly extending the defluidization time. However, the actual outcomes need to be verified by further experimental investigations.

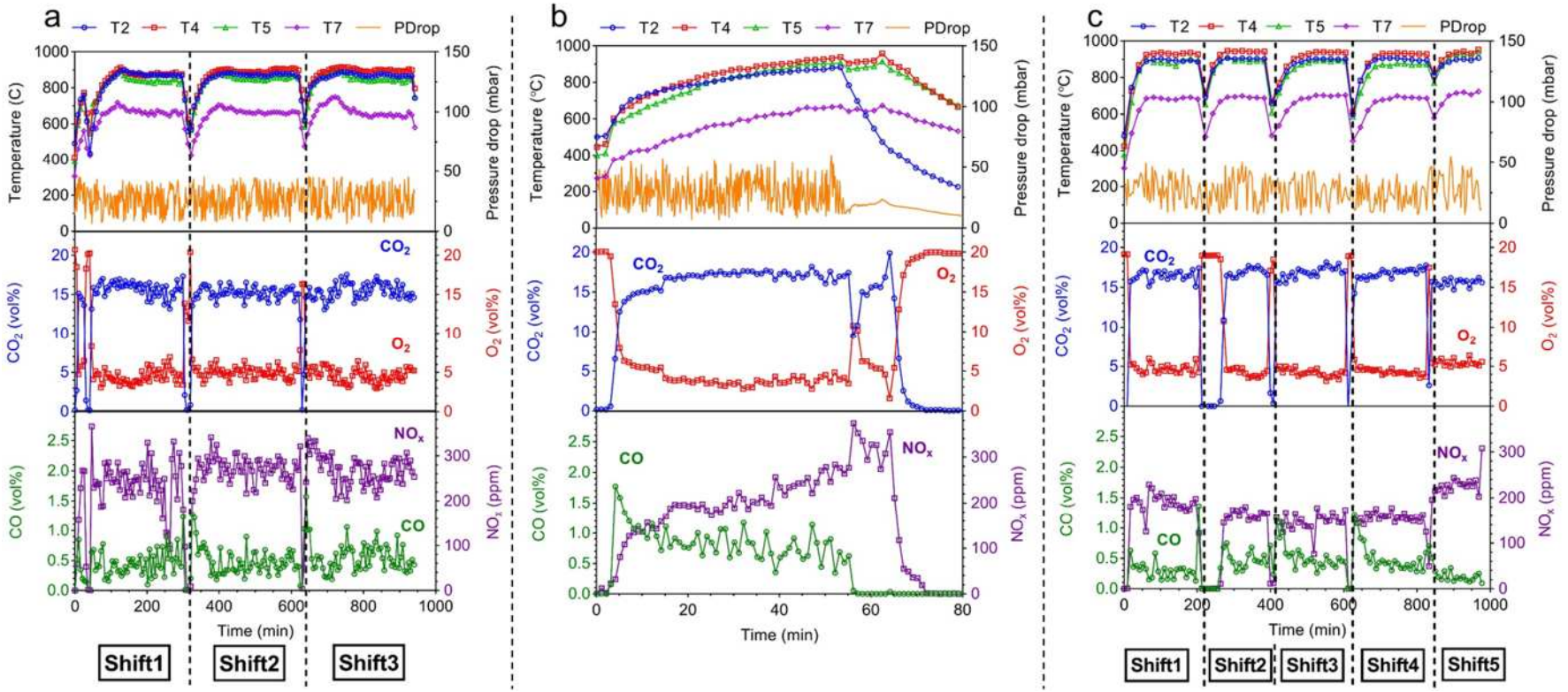

Fig. 4 Combustion profiles including bed temperature distributions, pressure drop, gas emissions of the three tests: (a) TB combustion test; (b) WS1 combustion test; (c) WS2 combustion test.

3.3.4 Phase identification of the fly ash and agglomerates

Fig. 5 shows the XRD spectrums of the fly ash and ground agglomerates from the three tests. The fly ash from TB combustion mainly consists of $CaCO_3$ and CaO (**Fig. 5** a), which have been widely acknowledged as effective additives in terms of anti-agglomeration. In the meantime, the agglomerates show high crystallinity with the main content of SiO_2. Potassium aluminosilicates and sodium-calcium phosphates are also detected in the agglomerates. Regarding the results of WS1 (**Fig. 5** b) and WS2 (**Fig. 5** c), the crystal phases in the agglomerates are almost identical, with a significant part of SiO_2 and a minor portion of potassium aluminosilicates. However, significant differences between the two wheat straw ashes can be observed: (1) WS1 derived fly ash has higher amorphous structures than WS2. This is caused by higher K content (KCl) in WS1 ash, and the resultant formation of low melting point K-rich eutectics during WS1 combustion. (2) Calcium silicates can be detected only in the WS2 derived fly ash, which is attributed to the interactions of the added lime and the Si content in the ash as well as the quartz bed. The high melting point calcium silicates can effectively hinder the accumulation of the molten phase K compounds, leading to a longer defluidization time.

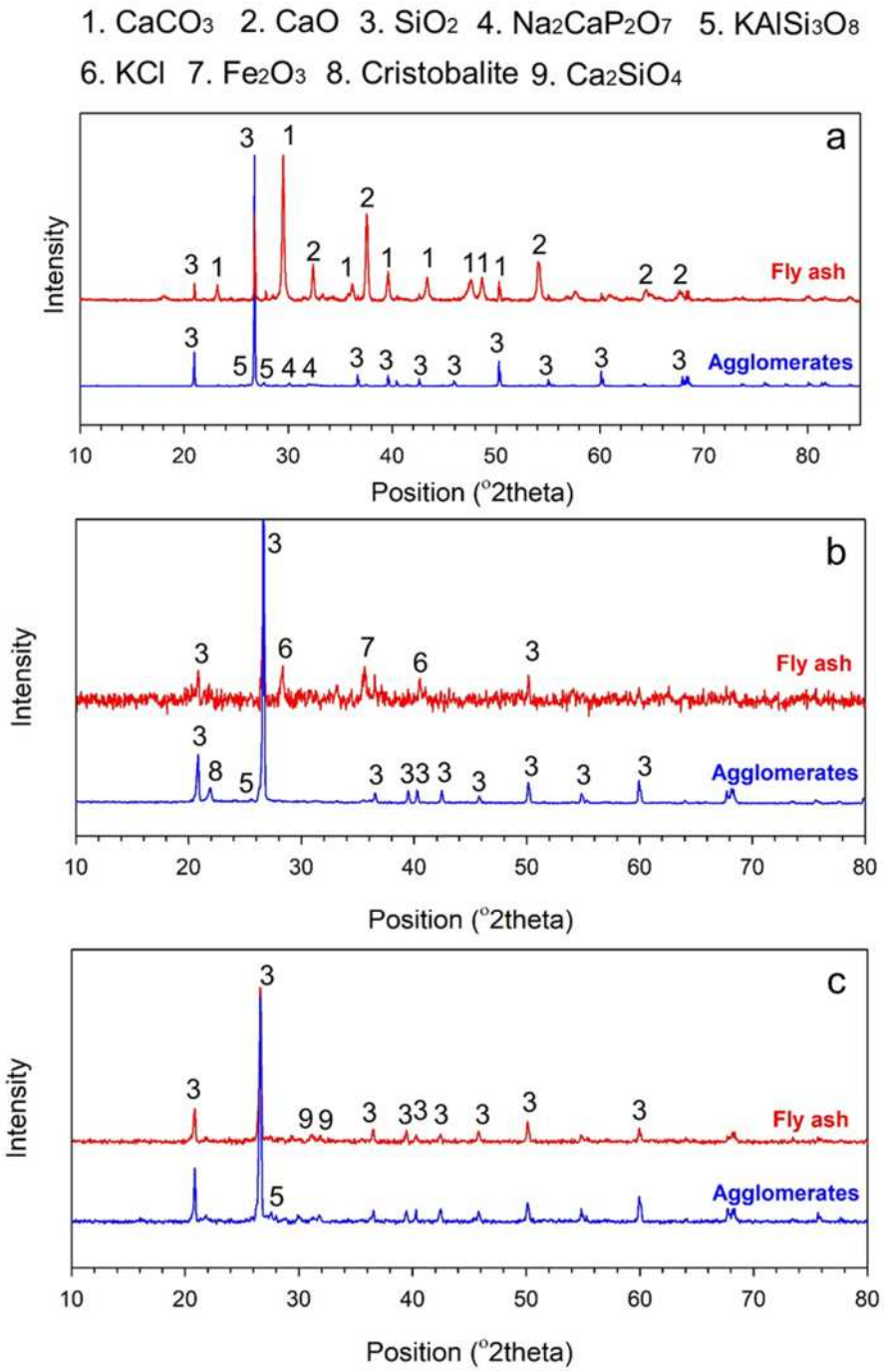

Fig. 5 XRD phase identification of the fly ash and agglomerates derived from the three tests: (a) TB; (b) WS1; (c) WS2.

3.3.5 SEM/EDX analysis on the cross-sections of the agglomerates

The cross-sections SEM/EDX analysis of the agglomerates is shown in **Fig. 6**. As seen, the bed particles in the TB derived agglomerates (**Fig. 6** a, b) are coated by a thin Ca-rich layer and connected with the "sticky" K-rich layer. After Shift 2 (**Fig. 6** a), the agglomerates size was still relatively small (1-2 mm), and the K-rich layer was in a dense structure with a few channels. In comparison, larger agglomerates (3-5 mm) were found after Shift 3 (**Fig. 6** b), and the K-rich layer tended to be a porous structure. Our previous study [22] has shown the cross-sections of the WS1 and WS2 derived agglomerates. A dense and homogeneous coating layer was observed in the WS1 agglomerates, mainly of K and Ca (**Fig. 6** c). WS2 agglomerates had multi-layers (K-rich inner layer and Ca-rich outer layer) coating around the bed particles (**Fig. 6** d). Moreover, the molten phases in the WS2 agglomerates had a floccus structure. These observations imply that the formation of the coating layer(s) is mostly dependent on the K/Ca ratio of the fuel ash: (1) When K/Ca >1, the agglomeration tendency is rapid due to the formation of the low melting point K-rich eutectics; (2) a 1.5 wt% lime addition to fuel decreased the K/Ca to ca.1. This considerably reduced the agglomeration propensity by forming a Ca-rich outer layer which successfully hindered further attachment of the molten K phases; (3) Firing TB with the K/Ca <<1, a thin Ca-rich coating layer was first developed around the bed particles, which effectively hindered the interactions between the molten phase potassium and the bed particles to form K-Si eutectics, thus significantly extending the defluidization time.

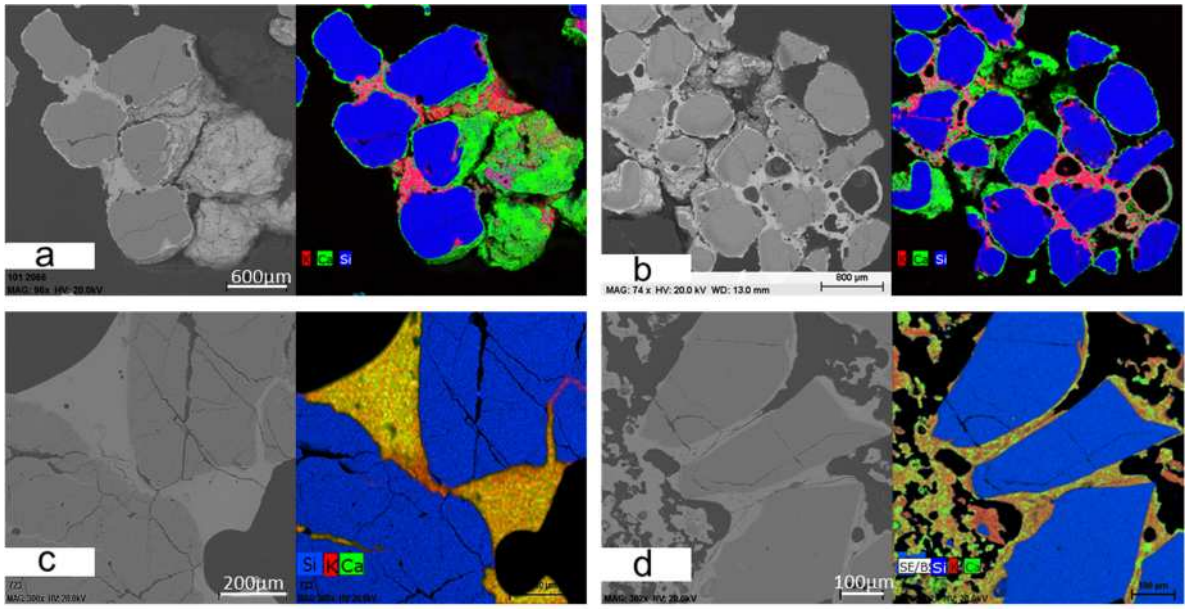

Fig. 6 SEM/EDX cross-section analysis with elemental mapping for selective agglomerates: (a) TB after Shift 2; (b) TB after Shift 3; (c) WS1; (d) WS2.

3.3.6 Elemental examination of the coating layers

As shown in **Fig. 6**, TB agglomerate has two different layers of coating. Therefore, to examine the elemental distribution in the coating layers, it is necessary to clarify the layers' consistency after each shift. **Fig. 7 a** presents the cross-section scanning of the agglomerates collected after each shift. It can be observed that a dense and homogeneous layer filled the gap between two adjacent bed particles while the outer layer covers the bed particles. When it comes to the agglomerate collected after Shift3, this fusion layer was formed by the interactions between the dense layer and the outer layer under the combustion temperature after long time operation [45].

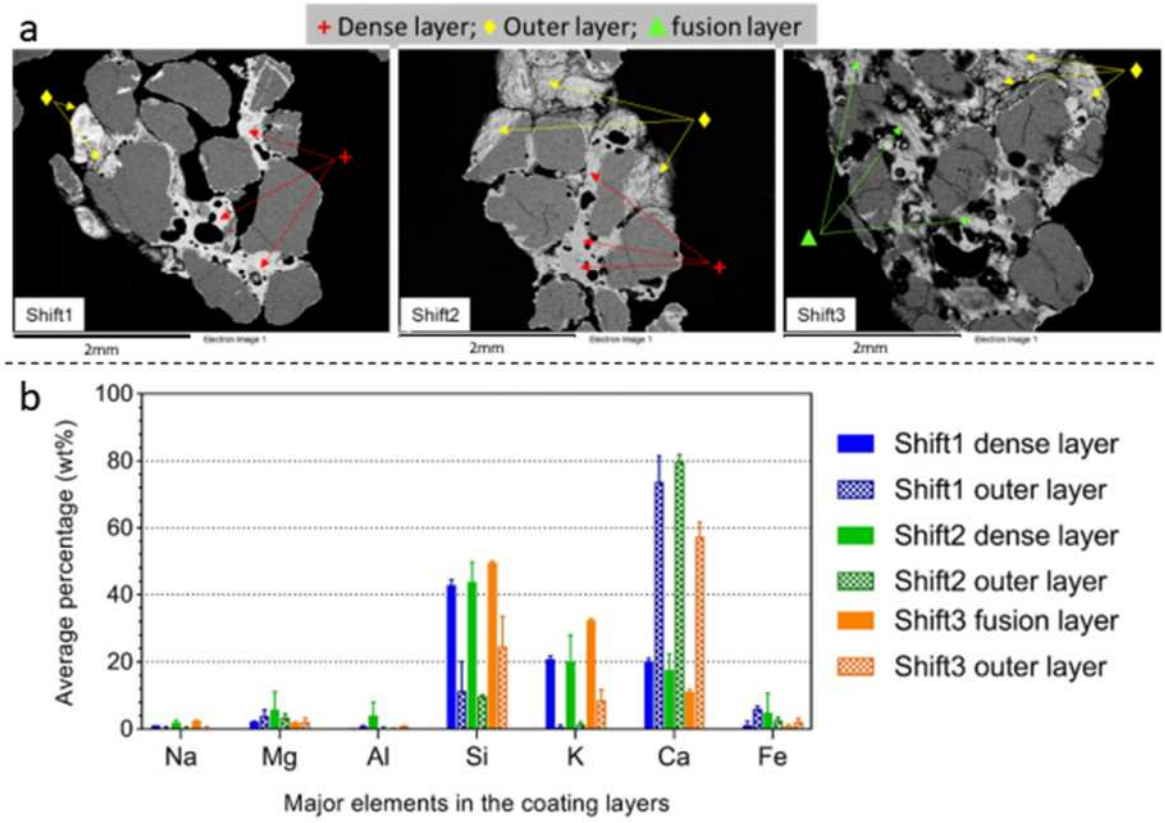

Fig. 7 Change of coating layers in the TB derived agglomerates collected after each Shift. (a) General morphology and classification of the coating layers; (b) SEM/EDX spot analysis on the coating layers

Considering the potential inconsistency of the coating layers, at least 10 points/squares were selected on both layers for the elemental examination, and the results are shown in **Fig. 7** b. Regarding the three major elements (Si, K, Ca), no noticeable difference can be found between the agglomerates collected from Shift1 and Shift2. However, the K concentration increased with a drop of Ca in the Shift3 fusion layer compared to the other dense layers. In the meantime, on the Shift3 outer layer, compared to the other outer layers, the K content increased with a decrease of Ca concentration. This demonstrates the interactions between the dense layer and outer layer in the Shift3-derived agglomerates and may finally lead to a K-rich fusion layer across the agglomerates [46]. Due to the limited fuel availability, the TB combustion experiment ended after three shifts. It should be worthwhile and interesting to

further investigate the time-dependent development of the fusion layer during the TB combustion in FB systems.

The ash elemental compositions and the elemental distribution of the coating layers of all three biomass fuels (TB, WS1 and WS2) were rearranged in the SiO_2 corner of the SiO_2-K_2O-CaO ternary diagram (**Fig. 8**) [47]. The 1.5wt% lime to fuel addition (WS2) can increase the fuel ash melting temperature and resulting in a higher temperature level for the formation of coating layers in the agglomerates. TB ash has an extremely high melting point due to the abundant Ca content. However, the accumulation of K content in the agglomerates can restrain the melting point down to ca. 900°C in the dense layer, which further develops into a fusion layer. On the other hand, the TB agglomerates' dense layer shows a melting point above 1500°C. This provides excellent potentials in the co-combustion of TB and WS1 in terms of mitigating the WS1 agglomeration tendency.

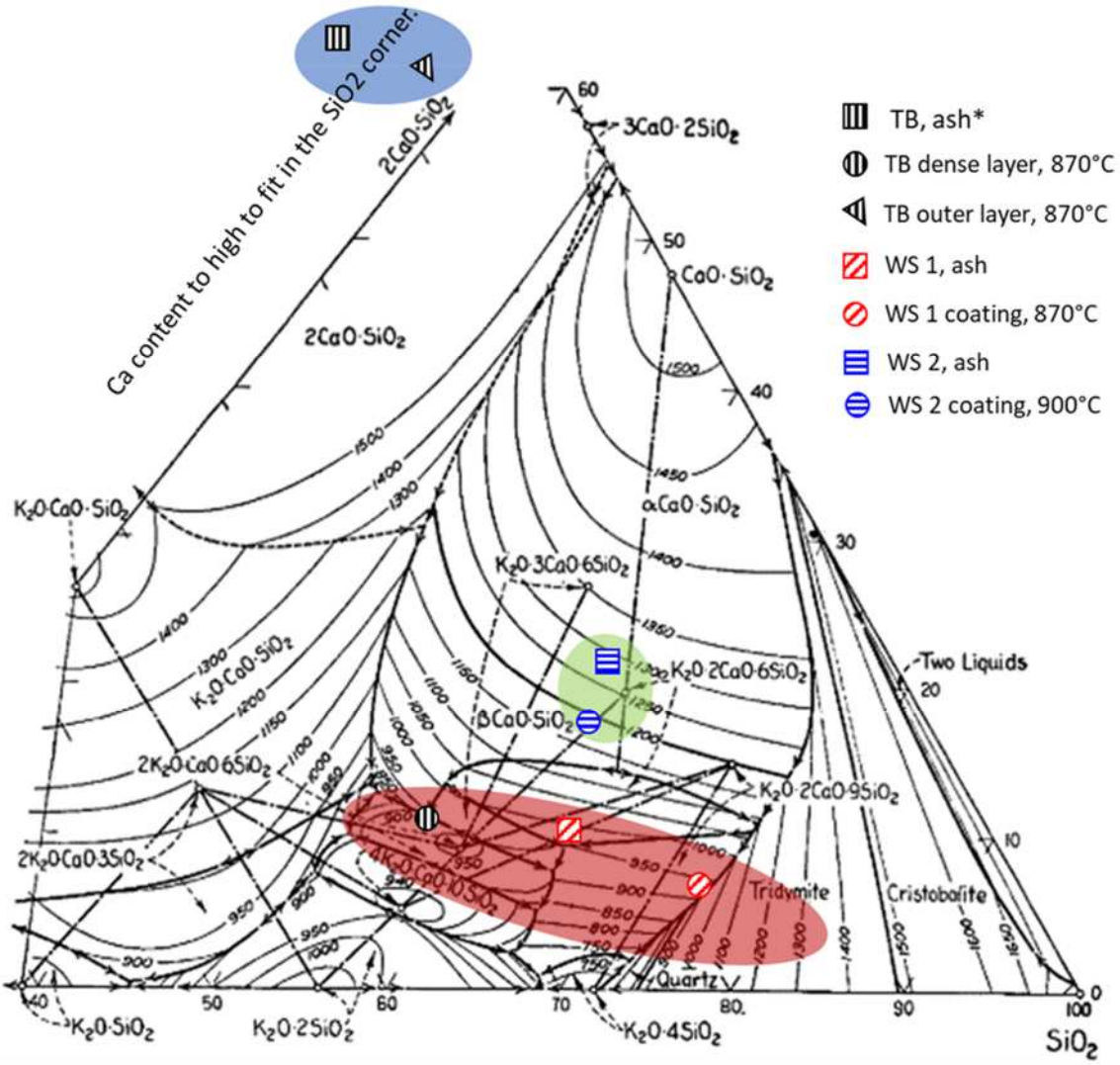

Fig. 8 SiO2 corner of the SiO2-K2O-CaO ternary diagram with the indications of elemental distribution of the coating layers.

3.4 Overall analysis of TB biorefinery

The tequila industry is constantly looking for new approaches to leverage its main wastes, i.e. vinasses and TB. Current practices to treat vinasses by AD in large factories has resulted in economic savings. However, successful treatments for TB are yet to be developed. This work provides comprehensive data about the experimental coupling of biochemical and thermochemical biorefinery platforms to convert TB to useful products. Regarding the biochemical platform, the two-stage AD showed that acid hydrolysates of TB can be used with or without detoxification to produce hydrogen and methane. Although more hydrogen is

produced with the detoxified hydrolysate, the total energy recovery is similar with both hydrolysates.

Pyrolysis of the residual fiber of the agave bagasse after acid pretreatment (H-TB) led to higher oil yields compared to TB, which is attributed to the lower ash content. Taking into account that during the acid pretreatment 40% of the solids are solubilized into the liquid fraction (hydrolysate) and the pyrolysis of H-TB at 500 and 750W yields approximately 50% oil, the recovered chemicals in the oil fraction (**Table 4**) represent bagasse yields up to 36.8 mg/g bagasse (for phenol, 2,6-dimethoxy). These chemical yields are additional to the 5 kJ/g bagasse obtained as hydrogen and methane from the biochemical route. It is important to highlight that all of the compounds shown in **Table 4** (furans, organic acids and phenolic compounds among others) have a potential use in the chemical industry and form part of the proposed biorefinery approach that aims to generate fuels and value-added products from TB.

Finally, concerning the BFB combustion tests, only the original bagasse was combusted due to the degradation of lignocellulose during acid hydrolysis, which apparently affected the pelletization process. Results from XRD, SEM/EDX analyses showed that the high $CaO/CaCO_3$ content in the TB ash substantially mitigated the agglomeration formation by forming a dense and stable Ca-rich coating layer around the bed particles. In the meantime, the outstanding anti-agglomeration ability of WS2 was due to the lime to fuel addition which is also a Ca-based additive. Therefore, it can be inferred that the co-combustion of TB and other problematic biomass fuels such as WS can lead to a stable combustion process with much lower agglomeration propensity. Moreover, considering TB combustion results in higher NOx emissions comparing to the combustion of WS1, co-firing TB with WS1 will also lead to lower NOx emissions, hence representing a better approach for valorizing TB in BFB systems.

4. Conclusions

This work has for the very first time demonstrated the feasibility of coupling the biochemical and thermochemical biorefinery platforms to valorize one of the main agro-industrial residues in Mexico, TB. The two-stage AD has showed that the detoxified acid hydrolysates from TB have great potential to produce hydrogen (doubling the hydrogen energy recovered comparing to the undetoxified hydrolysate). However, the total energy recovery, including the methanogenesis process, did not show significant differences between undetoxified or detoxified hydrolysates ($p \leq 0.05$), which was presumably due to the higher robustness of the methanogenic process and the biochemical barrier of the dark fermentation process to harvest high energy as hydrogen. Through the pyrolysis process, the remaining fiber of the acid pretreatment has showed its high potential to increase oil yields and reduce the ash and acetic acid formation due to the removal of calcium oxalates and hemicellulose during the acid pretreatment. This result highlights the advantages of the proposed technology to use the liquid fraction of the acid pretreatment of TB for two-stage AD and the remaining fiber for pyrolysis, obtaining energy recoveries up to 5 kJ/g bagasse and product yields up to 36.8 mg/g bagasse for phenol, 2,6-dimethoxy. Finally, although the combustion of the pretreated bagasse was not possible due to the difficulty to pelletize this biomass, the combustion test of the untreated TB in the fluidized bed system has showed that the co-combustion of the untreated TB with other problematic biomasses such as wheat straw potentially represents another alternative for valorization of TB. Overall, coupling the biochemical and thermochemical platforms for TB is hence considered as an innovative approach to simultaneously achieve the refinement of gaseous and liquid products, extraction of heat energy and disposal of the bio-waste from tequila industry.

Acknowledgements

This work was supported by a Newton Institutional Links grant, ID [332328157], under the Newton - CONACyT- SENER Partnership. The grant was co-funded by the UK Department of Business, Energy and Industrial Strategy (BEIS) and CONACyT- SENER (Sustentabilidad Energética project No. 291616) and delivered by the British Council.
Rios-Del Toro thanks CONACyT- SENER for postdoctoral fellowship under project 291616. Hetian Chi thanks the support from Power Distribution Network Multivariant Load Character Analysis and Prediction project No.52153820000J. The authors would also like to thank Dr. John Robinson and Dr. Mohamed Adam of the University of Nottingham for their help with the microwave pyrolysis tests and Dra. Alma Toledo for supervision of fermentation experiments. Tequila Herradura® is also acknowledged for supplying the agave bagasse.

References

[1] Abreu AA, Tavares F, Alves MM, Cavaleiro AJ, Pereira MA. Garden and food waste co-fermentation for biohydrogen and biomethane production in a two-step hyperthermophilic-mesophilic process. Bioresour Technol 2019;278:180–6. https://doi.org/10.1016/j.biortech.2019.01.085.

[2] CRT. Consejo Regulador del tequila-Statistical information 2020.

[3] Palomo-Briones R, López-Gutiérrez I, Islas-Lugo F, Galindo-Hernández KL, Munguía-Aguilar D, Rincón-Pérez JA, et al. Agave bagasse biorefinery: processing and perspectives. Clean Technol Environ Policy 2018;20:1423–41. https://doi.org/10.1007/s10098-017-1421-2.

[4] Perez-Pimienta JA, Poggi-Varaldo HM, Ponce-Noyola T, Ramos-Valdivia AC, Chavez-Carvayar JA, Stavila V, et al. Fractional pretreatment of raw and calcium oxalate-extracted agave bagasse using ionic liquid and alkaline hydrogen peroxide.

Biomass and Bioenergy 2016;91:48–55. https://doi.org/10.1016/j.biombioe.2016.05.001.

[5] Pérez-Pimienta JA, Vargas-Tah A, López-Ortega KM, Medina-López YN, Mendoza-Pérez JA, Avila S, et al. Sequential enzymatic saccharification and fermentation of ionic liquid and organosolv pretreated agave bagasse for ethanol production. Bioresour Technol 2017;225:191–8. https://doi.org/10.1016/j.biortech.2016.11.064.

[6] Montiel Corona V, Razo-Flores E. Continuous hydrogen and methane production from Agave tequilana bagasse hydrolysate by sequential process to maximize energy recovery efficiency. Bioresour Technol 2018;249:334–41. https://doi.org/10.1016/j.biortech.2017.10.032.

[7] Nissilä ME, Lay CH, Puhakka JA. Dark fermentative hydrogen production from lignocellulosic hydrolyzates - A review. Biomass and Bioenergy 2014;67:145–59. https://doi.org/10.1016/j.biombioe.2014.04.035.

[8] Arreola-Vargas J, Flores-Larios A, González-Álvarez V, Corona-González RI, Méndez-Acosta HO. Single and two-stage anaerobic digestion for hydrogen and methane production from acid and enzymatic hydrolysates of Agave tequilana bagasse. Int J Hydrogen Energy 2016;41:897–904. https://doi.org/10.1016/J.IJHYDENE.2015.11.016.

[9] Arreola-Vargas J, Ojeda-Castillo V, Snell-Castro R, Corona-González RI, Alatriste-Mondragón F, Méndez-Acosta HO. Methane production from acid hydrolysates of Agave tequilana bagasse: Evaluation of hydrolysis conditions and methane yield. Bioresour Technol 2015;181:191–9. https://doi.org/10.1016/j.biortech.2015.01.036.

[10] Breton-Deval L, Méndez-Acosta HO, González-Álvarez V, Snell-Castro R, Gutiérrez-Sánchez D, Arreola-Vargas J. Agave tequilana bagasse for methane production in batch and sequencing batch reactors: Acid catalyst effect, batch optimization and stability of

the semi-continuous process. J Environ Manage 2018;224:156–63. https://doi.org/10.1016/j.jenvman.2018.07.053.

[11] Farías-Sánchez JC, Velázquez-Valadez U, Vargas-Santillán A, Pineda-Pimentel MG, Mendoza-Chávez EA, Rutiaga-Quiñones JG, et al. Production of Fermentable Sugars and Hydrogen-Rich Gas from Agave tequilana Biomass. Bioenergy Res 2016;9:1015–22. https://doi.org/10.1007/s12155-016-9799-y.

[12] Parascanu MM, Sandoval-Salas F, Soreanu G, Valverde JL, Sanchez-Silva L. Valorization of Mexican biomasses through pyrolysis, combustion and gasification processes. Renew Sustain Energy Rev 2017;71:509–22. https://doi.org/10.1016/j.rser.2016.12.079.

[13] Sawatdeenarunat C, Nam H, Adhikari S, Sung S, Khanal SK. Decentralized biorefinery for lignocellulosic biomass: Integrating anaerobic digestion with thermochemical conversion. Bioresour Technol 2018;250:140–7. https://doi.org/10.1016/j.biortech.2017.11.020.

[14] Ghysels S, Acosta N, Estrada A, Pala M, De Vrieze J, Ronsse F, et al. Integrating anaerobic digestion and slow pyrolysis improves the product portfolio of a cocoa waste biorefinery. Sustain Energy Fuels 2020;4:3712–25. https://doi.org/10.1039/d0se00689k.

[15] Deng C, Kang X, Lin R, Murphy JD. Microwave assisted low-temperature hydrothermal treatment of solid anaerobic digestate for optimising hydrochar and energy recovery. Chem Eng J 2020;395:124999. https://doi.org/10.1016/j.cej.2020.124999.

[16] Pecchi M, Baratieri M. Coupling anaerobic digestion with gasification, pyrolysis or hydrothermal carbonization: A review. Renew Sustain Energy Rev 2019;105:462–75. https://doi.org/10.1016/j.rser.2019.02.003.

[17] Lü F, Hua Z, Shao L, He P. Loop bioenergy production and carbon sequestration of polymeric waste by integrating biochemical and thermochemical conversion processes: A conceptual framework and recent advances. Renew Energy 2018;124:202–11. https://doi.org/10.1016/j.renene.2017.10.084.

[18] Buitrón G, Carvajal C. Biohydrogen production from Tequila vinasses in an anaerobic sequencing batch reactor: Effect of initial substrate concentration, temperature and hydraulic retention time. Bioresour Technol 2010;101:9071–7. https://doi.org/10.1016/j.biortech.2010.06.127.

[19] Valdez-Guzmán BE, Rios-Del Toro EE, Cardenas-López RL, Méndez-Acosta HO, González-Álvarez V, Arreola-Vargas J. Enhancing biohydrogen production from Agave tequilana bagasse: Detoxified vs. Undetoxified acid hydrolysates. Bioresour Technol 2019;276:74–80. https://doi.org/10.1016/j.biortech.2018.12.101.

[20] Robinson J, Binner E, Saeid A, Al-Harahsheh M, Kingman S. Microwave processing of Oil Sands and contribution of clay minerals. Fuel 2014;135:153–61. https://doi.org/https://doi.org/10.1016/j.fuel.2014.06.057.

[21] Subagyono RRDJN, Qi Y, Jackson WR, Chaffee AL. Pyrolysis-GC/MS analysis of biomass and the bio-oils produced from CO/H2O reactions. J Anal Appl Pyrolysis 2016;120:154–64. https://doi.org/https://doi.org/10.1016/j.jaap.2016.05.001.

[22] Chi H, Pans MA, Sun C, Liu H. An investigation of lime addition to fuel as a countermeasure to bed agglomeration for the combustion of non-woody biomass fuels in a 20kWth bubbling fluidised bed combustor. Fuel 2019;240:349–61. https://doi.org/10.1016/j.fuel.2018.11.122.

[23] Yue GX, Yang HR, Lu JF, Zhang H. Latest Development of CFB Boilers in China BT - Proceedings of the 20th International Conference on Fluidized Bed Combustion. In: Yue G, Zhang H, Zhao C, Luo Z, editors., Berlin, Heidelberg: Springer Berlin

Heidelberg; 2010, p. 3–12.

[24] Channiwala SA, Parikh PP. A unified correlation for estimating HHV of solid, liquid and gaseous fuels. Fuel 2002;81:1051–63. https://doi.org/https://doi.org/10.1016/S0016-2361(01)00131-4.

[25] DuBois M, Gilles KA, Hamilton JK, Rebers PA, Smith F. Colorimetric Method for Determination of Sugars and Related Substances. Anal Chem 1956;28:350–6. https://doi.org/10.1021/ac60111a017.

[26] Pérez-Pimienta JA, Icaza-Herrera JPA, Méndoza-Pérez JA, González-Álvarez V, Méndez-Acosta HO, Arreola-Vargas J. Mild reaction conditions induce high sugar yields during the pretreatment of Agave tequilana bagasse with 1-ethyl-3-methylimidazolium acetate. Bioresour Technol 2019;275. https://doi.org/10.1016/j.biortech.2018.12.041.

[27] Palmqvist E, Hahn-Hägerdal B. Fermentation of lignocellulosic hydrolysates. I: Inhibition and detoxification. Bioresour Technol 2000;74:17–24. https://doi.org/10.1016/S0960-8524(99)00160-1.

[28] Alavi-Borazjani SA, Capela I, Tarelho LAC. Over-acidification control strategies for enhanced biogas production from anaerobic digestion: A review. Biomass and Bioenergy 2020;143:105833. https://doi.org/10.1016/j.biombioe.2020.105833.

[29] Monlau F, Sambusiti C, Barakat A, Quéméneur M, Trably E, Steyer JP, et al. Do furanic and phenolic compounds of lignocellulosic and algae biomass hydrolyzate inhibit anaerobic mixed cultures? A comprehensive review. Biotechnol Adv 2014;32:934–51. https://doi.org/10.1016/j.biotechadv.2014.04.007.

[30] Yin Q, Gu M, Wu G. Inhibition mitigation of methanogenesis processes by conductive materials: A critical review. Bioresour Technol 2020;317:123977. https://doi.org/10.1016/j.biortech.2020.123977.

[31] Łukajtis R, Hołowacz I, Kucharska K, Glinka M, Rybarczyk P, Przyjazny A, et al. Hydrogen production from biomass using dark fermentation. Renew Sustain Energy Rev 2018;91:665–94. https://doi.org/10.1016/j.rser.2018.04.043.

[32] Rittmann BE, McCarty PL. Environmental biotechnology: principles and applications. McGraw-Hill Education; 2001.

[33] Liñán-Montes A, De La Parra-Arciniega SM, Garza-González MT, García-Reyes RB, Soto-Regalado E, Cerino-Córdova FJ. Characterization and thermal analysis of agave bagasse and malt spent grain. J Therm Anal Calorim 2014;115:751–8. https://doi.org/10.1007/s10973-013-3321-y.

[34] Baêta BEL, Lima DRS, Adarme OFH, Gurgel LVA, Aquino SF de. Optimization of sugarcane bagasse autohydrolysis for methane production from hemicellulose hydrolyzates in a biorefinery concept. Bioresour Technol 2016;200:137–46. https://doi.org/10.1016/j.biortech.2015.10.003.

[35] Ridout AJ, Carrier M, Collard F-X, Görgens J. Energy conversion assessment of vacuum, slow and fast pyrolysis processes for low and high ash paper waste sludge. Energy Convers Manag 2016;111:103–14. https://doi.org/https://doi.org/10.1016/j.enconman.2015.12.043.

[36] Lin J-H, Chang Y-H, Hsu Y-H. Degradation of cotton cellulose treated with hydrochloric acid either in water or in ethanol. Food Hydrocoll 2009;23:1548–53. https://doi.org/https://doi.org/10.1016/j.foodhyd.2008.10.005.

[37] Subagyono DJN, Marshall M, Jackson WR, Chaffee AL. Pressurized thermal and hydrothermal decomposition of algae, wood chip residue, and grape marc: A comparative study. Biomass and Bioenergy 2015;76:141–57. https://doi.org/https://doi.org/10.1016/j.biombioe.2014.08.020.

[38] Oh S-J, Choi G-G, Kim J-S. Production of acetic acid-rich bio-oils from the fast

pyrolysis of biomass and synthesis of calcium magnesium acetate deicer. J Anal Appl Pyrolysis 2017;124:122–9. https://doi.org/https://doi.org/10.1016/j.jaap.2017.01.032.

[39] Jin F, Zhou Z, Kishita A, Enomoto H. Hydrothermal conversion of biomass into acetic acid. J Mater Sci 2006;41:1495–500. https://doi.org/10.1007/s10853-006-7493-8.

[40] Jin F, Zhou Z, Kishita A, Enomoto H, Kishida H, Moriya T. A New Hydrothermal Process for Producing Acetic Acid from Biomass Waste. Chem Eng Res Des 2007;85:201–6. https://doi.org/https://doi.org/10.1205/cherd06020.

[41] Budarin VL, Clark JH, Lanigan BA, Shuttleworth P, Breeden SW, Wilson AJ, et al. The preparation of high-grade bio-oils through the controlled, low temperature microwave activation of wheat straw. Bioresour Technol 2009;100:6064–8. https://doi.org/https://doi.org/10.1016/j.biortech.2009.06.068.

[42] Bartels M, Lin W, Nijenhuis J, Kapteijn F, van Ommen JR. Agglomeration in fluidized beds at high temperatures: Mechanisms, detection and prevention. Prog Energy Combust Sci 2008;34:633–66. https://doi.org/https://doi.org/10.1016/j.pecs.2008.04.002.

[43] Niu Y, Tan H, Hui S. Ash-related issues during biomass combustion: Alkali-induced slagging, silicate melt-induced slagging (ash fusion), agglomeration, corrosion, ash utilization, and related countermeasures. Prog Energy Combust Sci 2016;52:1–61. https://doi.org/https://doi.org/10.1016/j.pecs.2015.09.003.

[44] Chi H, Pans MA, Sun C, Liu H. An investigation of lime addition to fuel as a countermeasure to bed agglomeration for the combustion of non-woody biomass fuels in a 20kW<inf>th</inf> bubbling fluidised bed combustor. Fuel 2019;240. https://doi.org/10.1016/j.fuel.2018.11.122.

[45] He H, Boström D, Öhman M. Time Dependence of Bed Particle Layer Formation in Fluidized Quartz Bed Combustion of Wood-Derived Fuels. Energy & Fuels

2014;28:3841–8. https://doi.org/10.1021/ef500386k.

[46] He H, Skoglund N, Öhman M. Time-Dependent Layer Formation on K-Feldspar Bed Particles during Fluidized Bed Combustion of Woody Fuels. Energy & Fuels 2017;31:12848–56. https://doi.org/10.1021/acs.energyfuels.7b02386.

[47] Chen M, Hou X, Chen J, Zhao B. Phase Equilibria Studies in the SiO2-K2O-CaO System. Metall Mater Trans B 2016;47. https://doi.org/10.1007/s11663-016-0623-z.

Figure Captions

Fig. 1 Response surface for energy recovery from the two-stage anaerobic digestion of *A. tequilana* bagasse at different pH and COD concentrations. a) Undetoxified hydrolysate and b) detoxified hydrolysate.

Fig. 2 Solid, liquid and gas yields of different biomasses at different incident power levels during pyrolysis.

Fig. 3 Chromatogram of acetone soluble fractions from selective oil products: (a) TB at 500W; (b) H-TB at 500W; (c) WS at 500W.

Fig. 4 Combustion profiles including bed temperature distributions, pressure drop, gas emissions of the three tests: (a) TB combustion test; (b) WS1 combustion test; (c) WS2 combustion test.

Fig. 5 XRD phase identification of the fly ash and agglomerates derived from the three tests: (a) TB; (b) WS1; (c) WS2.

Fig. 6 SEM/EDX cross-section analysis with elemental mapping for selective agglomerates: (a) TB after Shift 2; (b) TB after Shift 3; (c) WS1; (d) WS2.

Fig. 7 Change of coating layers in the TB derived agglomerates collected after each Shift. (a) General morphology and classification of the coating layers; (b) SEM/EDX spot analysis on the coating layers

Fig. 8 SiO2 corner of the SiO2-K2O-CaO ternary diagram with the indications of elemental distribution of the coating layers.